

Alignment of non-spherical active particles in chaotic flows

M. Borgnino,¹ K. Gustavsson,² F. De Lillo,¹ G. Boffetta,¹ M. Cencini,^{3,*} and B. Mehlig²

¹*Dipartimento di Fisica and INFN, Università di Torino, via P. Giuria 1, 10125 Torino, Italy*

²*Department of Physics, Gothenburg University, 41296 Gothenburg, Sweden*

³*Istituto dei Sistemi Complessi, CNR, via dei Taurini 19, 00185 Rome, Italy and INFN, sez. Roma2 “Tor Vergata”*

We study the orientation statistics of spheroidal, axisymmetric microswimmers, with shapes ranging from disks to rods, swimming in chaotic, moderately turbulent flows. Numerical simulations show that rod-like active particles preferentially align with the flow velocity. To explain the underlying mechanism we solve a statistical model via perturbation theory. We show that such alignment is caused by correlations of fluid velocity and its gradients along particle paths combined with fore-aft symmetry breaking due to both swimming and particle nonsphericity. Remarkably, the discovered alignment is found to be a robust kinematical effect, independent of the underlying flow evolution. We discuss its possible relevance for aquatic ecology.

Active particles, such as motile microorganisms or artificial microswimmers, swim in a surrounding flow, either externally imposed or self-generated. In addition to transporting the active particles, velocity gradients change their swimming direction by exerting a shape-dependent torque [1, 2]. The complex interplay of flow advection, particle orientation and self-propulsion is fundamental to understand key processes in aquatic ecology [3–7], active matter modeling [8–10], and nano/micro-technology with application to drug delivery [11, 12].

Even simple laminar steady flows give rise to intriguing phenomena when combined with self-propulsion [13–16]. Rod-shaped motile bacteria are expelled by vortices [13] and display complex trajectories in pipe flows [14]. Microfluidic experiments in shear flows found that bacteria tumble in high shear regions, causing accumulation and chemotactic depletion [15]. In shear flows, a different tumbling mechanism traps bottom-heavy gyrotactic phytoplankton [17]. It has recently been found that individual bacteria in steady porous flow can orient their swimming direction with the local velocity leading to a strong enhancement (depletion) of the dispersion along (transverse to) the mean flow direction [18].

The behavior of active particles in unsteady flows is considerably less explored. Gyrotactic swimmers form small-scale fractal patches in turbulence [19–21], sampling different flow regions depending on their shape [21, 22]. Elongated swimmers, such as bacteria, remain quite homogeneously distributed in turbulent flows, while their orientation tends to nematically align with the vorticity [20, 23], similarly to elongated tracers [24, 25]. Much less is known about their orientation with respect to the flow velocity, which is key to light scattering in aquatic environments [26, 27], and for the encounter rates between organisms [4]. For instance, flow reorientation of elongated prey in the feeding currents of predators can strongly modify the capture rates [28]. Moreover, flow induced changes in the swimming direction can strongly alter chemotaxis, as found in steady shear flows [15].

In this Letter, aiming to fill this gap, we investigate

the dependence of the orientation statistics of active particles on their shape and speed in unsteady, moderately turbulent and stochastic flows. We find that swimming directions preferentially align with or against the local velocity field depending on the particle shape. Solving, by means of perturbative methods, the problem with a stochastic velocity field we trace back the origin of such an alignment to the correlation between flow velocity and its gradients along the particle path.

We consider dilute suspensions, disregarding any form of particle interaction. In this limit, we can neglect flow modifications induced by the active particles. We model a microswimmer as a small, neutrally buoyant, non-spherical, axisymmetric particle swimming with constant speed, v_s , in the direction \mathbf{n} of its symmetry axis. Assuming the particle size is smaller than the smallest flow scale, the particle center of mass \mathbf{x} evolves as [2]

$$\dot{\mathbf{x}} = \mathbf{u}(\mathbf{x}, t) + v_s \mathbf{n}, \quad (1)$$

$\mathbf{u}(\mathbf{x}, t)$ being the fluid velocity at the particle position. Particle orientation rotates in response to velocity gradients, according to Jeffery’s dynamics [1]

$$\dot{\mathbf{n}} = [\mathbb{O}(\mathbf{x}, t) + \Lambda \mathbb{S}(\mathbf{x}, t)] \mathbf{n} - \Lambda [\mathbf{n} \cdot \mathbb{S}(\mathbf{x}, t) \mathbf{n}] \mathbf{n} \equiv \mathbf{J}(\mathbf{n}), \quad (2)$$

where \mathbb{O} and \mathbb{S} are the antisymmetric (vorticity) and symmetric (strain) components of the velocity gradient matrix $\mathbb{A}_{ij} = \partial u_i / \partial x_j$, respectively. For $v_s = 0$, the above dynamics reproduces that of spheroidal tracers that have recently gathered much attention [24, 25, 29].

The dynamics is controlled by two dimensionless numbers. The first is the *shape parameter* $\Lambda = (a^2 - b^2)/(a^2 + b^2)$ (a and b being the particle size along and perpendicular to the symmetry axis): $\Lambda = 0$ for spheres, and $\Lambda = \pm 1$ for infinitely slender rods and thin platelets, respectively. The second is the *swimming number* $\Phi = v_s \tau / \ell$, ℓ and τ being the flow typical scale and time, discussed below. For $\Lambda > 0$, Eqs. (1-2) represent a minimal model for a smooth swimming (not tumbling) bacterium [15, 16]. Rotational diffusivity in Eq. (2) is neglected to reduce the number of parameters.

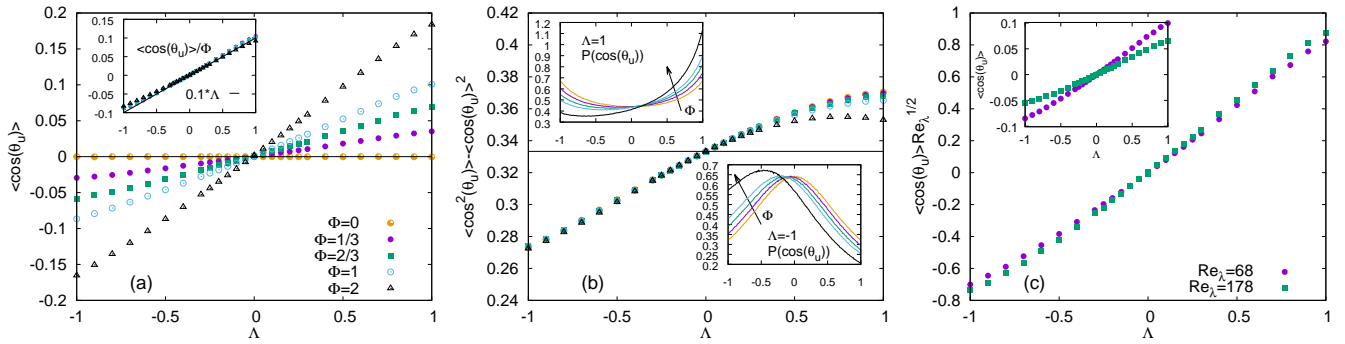


FIG. 1. (Color online) Statistics of particle orientation with respect to the flow velocity, obtained from DNS of the NSE (3), as a function of the particle shape parameter Λ , for different swimming number Φ . (a) $\langle \cos \theta_u \rangle$ vs Λ for different Φ at $\text{Re}_\lambda \approx 68$. Inset: $\langle \cos \theta_u \rangle / \Phi$ vs Λ , the solid line represents a linear best fit. (b) Variance of $\cos \theta_u$ vs Λ for different Φ . Top (bottom) inset shows the PDF of $\cos \theta_u$ for rod- (disk-) like particles with Φ from 0 to 2 along the arrows. (c) Same as panel (a) for $\Phi = 1$ and $\text{Re}_\lambda = 68$ and 178 . Main panel shows $\langle \cos \theta_u \rangle \text{Re}_\lambda^{1/2}$ vs Λ . Inset shows the non-rescaled data. Data are obtained by averaging over 100 snapshots, separated by about half large-scale eddy turnover time, with up to $3 \cdot 10^5$ particles for each Λ and Φ values.

We start considering homogeneous, isotropic turbulent flows obtained by direct numerical simulations (DNS) of the Navier-Stokes equations (NSE)

$$\partial_t \mathbf{u} + \mathbf{u} \cdot \nabla \mathbf{u} = -\nabla p + \nu \Delta \mathbf{u} + \mathbf{F}, \quad (3)$$

where fluid density is scaled to unity, pressure p ensures flow incompressibility ($\nabla \cdot \mathbf{u} = 0$) and ν is the viscosity. The stirring force \mathbf{F} is an incompressible, zero-mean, temporally uncorrelated Gaussian random field, injecting kinetic energy at large scales at a rate ϵ to generate a statistically steady state. We solve Eqs. (3), by means of a 2/3-dealiased pseudospectral solver with a 2nd order Runge-Kutta scheme, in a triply periodic domain with $N^3 = 128^3 - 512^3$ mesh points. The Kolmogorov length, $\eta = (\nu^3/\epsilon)^{1/4}$, is larger than the grid spacing and the time step much smaller than the Kolmogorov timescale, $\tau_\eta = (\nu/\epsilon)^{1/2}$, to well resolve the small scales dynamics. Velocity and its gradients at particle positions, needed to integrate Eqs. (1-2), are obtained via a third order interpolation scheme. The swimming number is defined as $\Phi = v_s \tau_\eta / \eta = v_s / u_\eta$, u_η being the Kolmogorov velocity. We consider moderately turbulent flows, with Taylor-scale Reynolds number $\text{Re}_\lambda = \sqrt{15} u_{\text{rms}} / (\nu \epsilon)^{1/2} \approx 70-180$.

For non-spherical particles we find a remarkable alignment of the swimming direction with the local velocity field quantified by the statistics of the angle, θ_u , between \mathbf{n} and \mathbf{u} . Figure 1a shows that $\langle \cos \theta_u \rangle \neq 0$ provided the particle is not spherical ($\Lambda \neq 0$) and active ($\Phi > 0$) ($\langle \dots \rangle$ denotes the average over particle positions). Data suggest that $\langle \cos \theta_u \rangle \propto \Lambda \Phi$ (inset of Fig. 1a) at least for small Φ and Λ , with some deviations from linear behavior for $|\Lambda| \rightarrow 1$. We remark that such alignment depends on the particle shape: it is “polar-like” for elongated particles ($\Lambda > 0$) and anti-polar for disk-like ones ($\Lambda < 0$). Thus, on average, rod-like particles swim along the underlying flow velocity while disk-like ones against it.

The variance of $\cos \theta_u$ (Fig. 1b) displays a non-trivial dependence on Λ while it is almost insensitive to Φ , except around $\Lambda \rightarrow 1$, where it slightly decreases with Φ . The different behavior for disk-(rod)-like particles reflects qualitative differences in the probability density function (PDF) of $\cos \theta_u$. For disks (bottom inset), the PDF of $\cos \theta_u$ displays a peak that gradually moves from 0 (swimming normal to velocity) to negative values at increasing Φ . Conversely, for rods (top inset) the PDF is bimodal at ± 1 for $\Phi = 0$ with a progressive bias in favor of +1 peak at increasing Φ . Thus elongated particles ($\Lambda > 0$) align with the local fluid velocity for any Φ but the alignment changes from nematic to polar upon increasing Φ .

To rationalize the above observations, we now consider a statistical model for the velocity field, $\mathbf{u}(\mathbf{x}, t)$, which allows for analytical treatments. As detailed in [30] (see Sect. I.A in the Supplemental Material (SM)[31]), we consider a (single scale, single time) random Gaussian velocity field parameterized by typical flow speed u_f with correlation length, ℓ_f , and time, τ_f . We introduce the additional dimensionless number, namely the Kubo number $\text{Ku} = u_f \tau_f / \ell_f$, quantifying how rapidly the fluid velocity fluctuates. Figure 2 displays the statistics of alignment obtained from a numerical simulation of the stochastic model. The agreement with the results obtained in turbulent flows (Fig. 1) is remarkable, demonstrating that the alignment is a robust *kinematical* phenomenon, i.e. independent of the dynamics producing the flow. This is in contrast with the known alignment observed for elongated swimmers with the local vorticity $\boldsymbol{\omega}(\mathbf{x}, t) = \nabla \times \mathbf{u}(\mathbf{x}, t)$ [20, 23], which is absent in the stochastic flow. Indeed, the origin of alignment with vorticity is *dynamical* as discussed in [25] for elongated tracers and stems from the formal similarity of Eq. (2) for $\Lambda = 1$ with the Lagrangian dynamics of vorticity. See Sect. IV in SM [31] for further considerations.

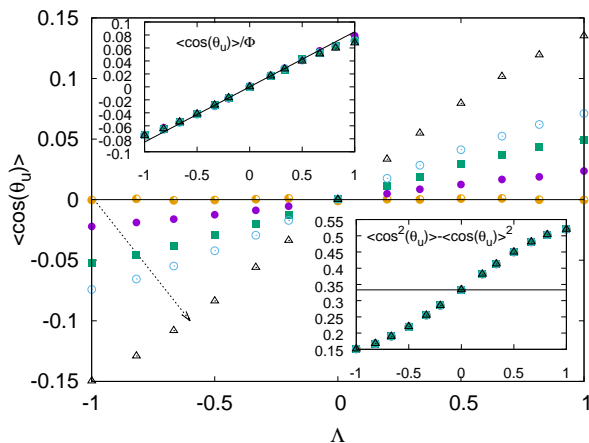


FIG. 2. (Color online) Statistics of orientation obtained by simulations of the stochastic model for $Ku = 10$. Main panel: $\langle \cos \theta_u \rangle$ vs Λ for different swimming speeds, $\Phi_s = 0, 0.3, 0.7, 1, 2$ as indicated by the arrow, Top inset: $\langle \cos \theta_u \rangle / \Phi_s$ vs Λ . Bottom inset: variance of $\cos \theta_u$.

The advantage of the stochastic model is that it allows for reaching an analytical understanding of the basic mechanism for the alignment. In particular, we study the statistics of $\langle \mathbf{n} \cdot \mathbf{u} \rangle$ instead of $\langle \mathbf{n} \cdot \mathbf{u} \rangle / |\mathbf{u}| = \cos \theta_u$, as they convey the same qualitative information on alignment (Fig. 3), and are easier to handle. The main difficulty in analyzing Eqs. (1-2) lies in their non-linear dependence on the particle position. Such a hindrance can be overcome in perturbation theory, by iteratively improving approximations for the particle trajectory, a technique successfully employed to analyze inertial particles [30] and gyrotactic swimmers [21]. This corresponds to an expansion in the Kubo number [30].

In the following we briefly outline the main steps, detailed calculations can be found in Sect. II.A of SM [31]. To apply perturbation theory we introduce dimensionless variables with $t = t' \tau_f$, $x = x' \ell_f$, and $u = u' u_f$, in terms of which Eqs. (1-2) read: $\dot{\mathbf{x}}' = Ku \mathbf{u}' + \Phi_s \mathbf{n}$ and $\dot{\mathbf{n}} = Ku \mathbf{J}'(\mathbf{n})$, with swimming number $\Phi_s = v_s \tau_f / \ell_f$. The above equations imply that, for $Ku=0$, the particle paths are simply $\mathbf{x}'_{t'} = \mathbf{x}'_0 + \Phi_s \mathbf{n}_0 t'$, where (d) denotes the zeroth order (deterministic) solution. We can now write $\mathbf{x}'_{t'} = \mathbf{x}'_{t'}^{(d)} + \delta \mathbf{x}_{t'}$ and expand Eqs. (1-2) to the desired order in $\delta \mathbf{x}_{t'}$, leading to an expansion in Ku at fixed Φ_s [30, 31]. The result is then averaged using the known correlation functions of the (Gaussian) velocity field and its derivatives. Using flow isotropy, homogeneity, and incompressibility, the stationary-state average of the scalar product between \mathbf{n} and \mathbf{u} takes the (dimensional) form:

$$\langle \mathbf{n} \cdot \mathbf{u} \rangle = -d\Lambda \int_0^t dt_1 \partial_R C_{\parallel}(R, t_1) \Big|_{\mathbf{R}=\mathbf{x}_{t_1}^{(d)}}, \quad (4)$$

d being the spatial dimension and $R = |\mathbf{R}|$. For the stochastic flow, the longitudinal velocity covariance takes the form $C_{\parallel}(R, t) \equiv \langle (\mathbf{u}(\mathbf{x} + \mathbf{R}, t) \cdot \hat{\mathbf{R}})(\mathbf{u}(\mathbf{x}, 0) \cdot \hat{\mathbf{R}}) \rangle =$

$\exp[-(R^2/2\ell_f^2 + |t|/\tau_f)]/d$. Substituting it in Eq. (4) and using $\mathbf{x}_{t_1}^{(d)} = \Phi_s \mathbf{n}_0 t_1$, the integral can be easily computed (see Sect. II.C in SM [31]), yielding for $\Phi_s \ll 1$

$$\langle \mathbf{n} \cdot \mathbf{u} \rangle \simeq u_f \Lambda Ku \Phi_s, \quad (5)$$

which agrees well with the numerically obtained scaling of $\cos \theta_u$ in terms of Λ and Φ (inset of Fig. 1a and Fig. 2). Figure 3a shows that, for $Ku \ll 1$, statistical-model simulations perfectly agrees with the theoretical prediction.

Neglecting vorticity in (2), in the limit of small swimming speeds and $|\Lambda|$, an expansion similar to that used in [32] can be performed yielding (see Sect. V in SM [31])

$$\langle \mathbf{n} \cdot \mathbf{u} \rangle = \frac{2\Lambda v_s}{d+2} \int_0^t dt_1 t_1 \text{Tr} \langle \mathbb{S}(\mathbf{x}_{t_1}^L, t_1) \mathbb{S}(\mathbf{x}_0^L, 0) \rangle, \quad (6)$$

which expresses $\langle \mathbf{n} \cdot \mathbf{u} \rangle$ in terms of the correlation function of the strain along Lagrangian trajectories, \mathbf{x}_t^L , i.e. corresponding to the dynamics (1) with $v_s = 0$. Note that the above expression, being free from any assumption on the flow statistics, only requires v_s and Λ to be small and should therefore be valid for generic flows and Kubo numbers (see Sect. V in SM [31]). We measured $\text{Tr} \langle \mathbb{S}(\mathbf{x}_t^L, t) \mathbb{S}(\mathbf{x}_0^L, 0) \rangle$ along Lagrangian trajectories in DNS and numerically computed the integral in (6) obtaining a prediction for $\langle \mathbf{n} \cdot \mathbf{u} \rangle$ that agrees well with the numerical data, at least for not too large Φ and Λ (Fig. 3b).

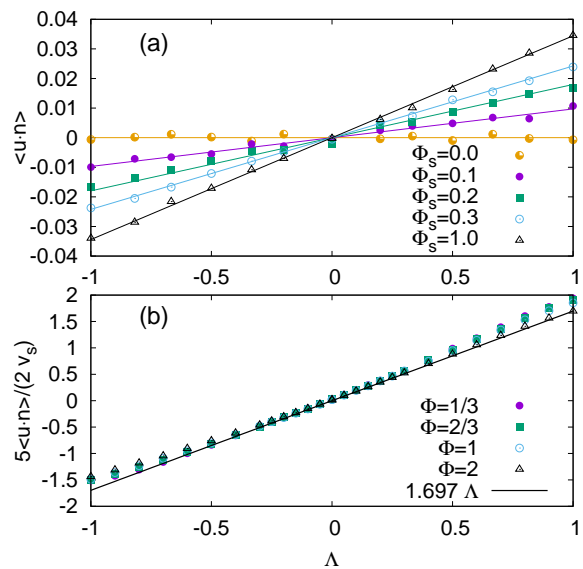


FIG. 3. (Color online) Comparison between theoretical predictions and simulations for both the statistical model and DNS. (a) $\langle \mathbf{n} \cdot \mathbf{u} \rangle$ vs Λ for different Φ_s obtained numerically for the statistical model with $Ku = 0.1$ (symbols) compared with the theoretical prediction (4) (solid lines). (b) $5\langle \mathbf{n} \cdot \mathbf{u} \rangle / (2v_s)$ vs Λ for different $\Phi = v_s/u_\eta$ for the DNS at $Re_\lambda \approx 68$. The solid line represents the prediction (6), 1.697Λ with the numerical prefactor was numerically obtained evaluating the strain correlation function along tracer trajectories.

The physical meaning of Eq. (4) is as follows: The alignment results from the non-zero correlation between velocity and its gradients at different times (this is $\partial_R C_{\parallel}(R, t-t_1)$). However, such correlation brings a non-zero contribution only if swimming ($v_s \neq 0$) and non-sphericity ($\Lambda \neq 0$) are present. Essentially swimming in the instantaneous direction breaks the fore-aft symmetry and the dynamics of \mathbf{n} is no longer identical to the dynamics of $-\mathbf{n}$, leading to a non-zero value for $\langle \mathbf{n} \cdot \mathbf{u} \rangle$ (see Sect. II.C in SM [31] for further considerations). For the second moment, the situation is different, to order Ku^2 and for $\Phi \ll 1$ we find (see Sect. III in SM [31])

$$\langle (\mathbf{n} \cdot \mathbf{u})^2 \rangle / u_f^2 \sim \frac{1}{d} + \frac{\text{Ku}^2 \Lambda}{d} + \frac{\text{Ku}^2 \Phi^2 \Lambda}{2d} (2d\Lambda - 11), \quad (7)$$

which depends on Λ also for non-swimming particles, as confirmed by simulations.

In the statistical model, there is a single time scale for both velocity and its gradients. Conversely, in turbulence there is a time scale separation between them controlled by $\text{Re}_\lambda \approx T/\tau_\eta$ (T being the integral timescale). Thus, for strong turbulence, the dynamics of the orientation, ruled by velocity gradients, will vary over time scales ($\sim \tau_\eta$) much faster than the correlation time of the velocity ($\sim T$), possibly depleting the alignment. This is confirmed in the inset of Fig. 1c showing that $\langle \cos \theta_u \rangle \sim \text{Re}_\lambda^{-1/2}$. This $\text{Re}_\lambda^{-1/2}$ scaling can be rationalized as follows. The statistical model calculations predict that, for given Ku , alignment only depends on Λ and Φ_s . Thus we need to map the swimming parameter of the model on that used in turbulence. Following Ref. [21] (see also Sect. I.A in SM [31]) the statistical model length (ℓ_f) and time (τ_f) scales should be related to the Taylor length scale, $\lambda \propto u_{\text{rms}} \tau_\eta$ and τ_η , respectively, being the scales relevant to the gradients. Therefore, the swimming number to be used to compare DNS with the statistical model should be based on the r.m.s. velocity, indeed $\Phi_s = v_s \tau_\eta / \lambda \propto v_s / u_{\text{rms}}$ (see also [22] for related considerations), while we used $\Phi = v_s / u_\eta$. The two swimming numbers are thus related by $\Phi_s \propto \Phi (u_\eta / u_{\text{rms}}) \propto \text{Re}_\lambda^{-1/2} \Phi$, which explains the scaling observed in Fig. 1c. DNS results (not shown) confirm that for fixed Φ_s the alignment statistics is independent of Re_λ . Thus, alignment can be important also for high Re_λ flows provided the particle speed is a fraction of the large scale velocity. Such large speeds can be attained by swimmers larger than the Kolmogorov scale, for which Eqs. (1-2) may still be valid, provided the Stokes number defined on the particle scale is small enough, as recently found in finite-size fibers [33].

In general, alignment is expected to be important whenever turbulence is moderate, i.e. in velocity fields with not too separated scales of motion, as commonly found in environmental, laboratory and biomedical fluids. In marine environments with calm water the Kolmogorov

velocity is in the order of $u_\eta \approx 300 - 1000 \mu\text{m}/\text{s}$ [4] while bacterial speeds range in $v_s \approx 30 - 300 \mu\text{m}/\text{s}$ [34] consequently $\Phi \approx 0.05 - 1$. Hence, depending on the Reynolds number, alignment can be substantial. Alignment could be relevant to models for light scattering in aquatic environments [26, 27] especially considering that most of motile microorganisms are elongated [26], and for the encounter rates of aquatic microorganisms [4, 28]. Further, analogously to the findings in steady shear flows [15], flow reorientation may alter the chemotactic efficiency. For instance, flow-induced alignment could be particularly relevant to marine bacteria, many of which perform a run-reverse cycle in which the orientation is unchanged while the swimming velocity is reversed [35].

Preliminary studies, to be discussed elsewhere, show that alignment persists also in the presence of a non-homogeneous mean flow. In this case, alignment may dramatically impact the dispersal properties along and transverse to the mean flow similarly to what is observed in steady porous flows [18], with implications for groundwater filtration and remediation, and biomedical fluids. Remarkably, the experiments in [18] demonstrated preferential alignment of the bacterial swimming direction with the local flow in analogy with our findings. It would be then interesting to study alignment in the limit of steady flows, i.e. in the $\text{Ku} \rightarrow \infty$ limit, to understand whether the physical mechanism for alignment is the same of that we found in unsteady flows. This is however beyond the scope of the present Letter.

Finally, we observe that nontrivial correlations between flow velocity and individual bacterial orientation have been reported in dense suspensions [36, 37], where the self-generated flow is in the order of $\sim 50 - 100 \mu\text{m}/\text{s}$ with correlation length of $30 - 100 \mu\text{m}$, while bacteria swim at speed $\sim 15 - 20 \mu\text{m}/\text{s}$ with a size of $\sim 2 \mu\text{m}$ [36, 38]. With swimming numbers in the order of $\approx 0.15 - 0.4$, it is tempting to speculate that the alignment here discussed could be an important effect. However, this needs to be tested because steric and hydrodynamic interactions, here neglected, play a major role.

Summarizing, we found that (disk-)rod-like active particles swimming in a moderately turbulent background flow tend to preferentially align their swimming direction (anti) parallel to the underlying flow velocity. We showed that such an alignment has a kinematical origin and analytically found its roots in the time correlations between velocity and its gradients along particle paths together with the fore-aft symmetry breaking induced by swimming. Our study expands on the possible non-trivial behaviors of microswimmers in an external flow [5, 7] from the simple cases of pipe or shear flows [13, 14] to realistic unsteady turbulent and chaotic flows.

We acknowledge useful discussions with R. Stocker. MB, GB and FDL acknowledge support by the *Departments of Excellence* grant (MIUR). BM and KG acknowledge Knut and Alice Wallenberg Foundation,

grant no. KAW 2014.0048, and Vetenskapsrådet, grant no. 2017-3865. CINECA is acknowledged for computing resources, within the INFN-Cineca agreement INF18-fldturb and the Iskra-C GyATuS grant.

* Corresponding author; massimo.cencini@cnr.it

- [1] G. B. Jeffery, Proc. Royal Soc. Lond. Ser. A **102**, 161 (1922).
- [2] T. J. Pedley and J. O. Kessler, Proc. Royal Soc. Lond. Ser. B **231**, 47 (1987).
- [3] R. H. Luchsinger, B. Bergersen, and J. G. Mitchell, Biophys. J. **77**, 2377 (1999).
- [4] T. Kiørboe, *A mechanistic approach to plankton ecology* (Princeton University Press, 2008).
- [5] R. Rusconi and R. Stocker, Curr. Opin. Microbiol. **25**, 1 (2015).
- [6] J. R. Taylor and R. Stocker, Science **338**, 675 (2012).
- [7] J. S. Guasto, R. Rusconi, and R. Stocker, Annu. Rev. Fluid Mech. **44**, 373 (2012).
- [8] M. C. Marchetti, J.-F. Joanny, S. Ramaswamy, T. B. Liverpool, J. Prost, M. Rao, and R. A. Simha, Rev. Mod. Phys. **85**, 1143 (2013).
- [9] C. Bechinger, R. Di Leonardo, H. Löwen, C. Reichhardt, G. Volpe, and G. Volpe, Rev. Mod. Phys. **88**, 045006 (2016).
- [10] J. Elgeti, R. G. Winkler, and G. Gompper, Rep. Progr. Phys. **78**, 056601 (2015).
- [11] R. Dreyfus, J. Baudry, M. L. Roper, M. Fermigier, H. A. Stone, and J. Bibette, Nature **437**, 862 (2005).
- [12] B. J. Nelson, I. K. Kaliakatsos, and J. J. Abbott, Annu. Rev. Biomed. Engin. **12**, 55 (2010).
- [13] C. Torney and Z. Neufeld, Phys. Rev. Lett. **99**, 078101 (2007).
- [14] A. Zöttl and H. Stark, Phys. Rev. Lett. **108**, 218104 (2012), Europ. Phys. J. E **36**, 41 (2013).
- [15] R. Rusconi, J. S. Guasto, and R. Stocker, Nature Phys. **10**, 212 (2014).
- [16] G. Junot, N. Figueroa-Morales, T. Darnige, A. Lindner, R. Soto, H. Auradou, and E. Clément, EPL **126**, 44003 (2019).
- [17] W. M. Durham, J. O. Kessler, and R. Stocker, Science **323**, 1067 (2009).
- [18] A. Dehkarghani, N. Waisbord, J. Dunkel, and J. S. Guasto, Proc. Nat. Acad. Sci. **116**, 11119 (2019).
- [19] W. M. Durham, E. Climent, M. Barry, F. De Lillo, G. Boffetta, M. Cencini, and R. Stocker, Nature Commu. **4**, 2148 (2013).
- [20] C. Zhan, G. Sardina, E. Lushi, and L. Brandt, J. Fluid Mech. **739**, 22 (2014).
- [21] K. Gustavsson, F. Berglund, P. R. Jonsson, and B. Mehlig, Phys. Rev. Lett. **116**, 108104 (2016).
- [22] M. Borgnino, G. Boffetta, F. De Lillo, and M. Cencini, J. Fluid Mech. **856** (2018).
- [23] N. Pujara, M. Koehl, and E. Variano, J. Fluid Mech. **838**, 356 (2018).
- [24] G. A. Voth and A. Soldati, Annu. Rev. Fluid Mech. **49**, 249 (2017).
- [25] A. Pumir and M. Wilkinson, New J. Phys. **13**, 093030 (2011).
- [26] W. E. Clavano, E. Boss, and L. Karp-Boss, Ocean. Mar. Biol. **45**, 1 (2007).
- [27] Marcos, J. R. Seymour, M. Luhan, W. M. Durham, J. G. Mitchell, A. Macke, and R. Stocker, Proc. Nat. Acad. Sci. **108**, 3860 (2011).
- [28] A. W. Visser and P. R. Jonsson, J. Plankton Res. **22**, 761 (2000).
- [29] M. Byron, J. Einarsson, K. Gustavsson, G. Voth, B. Mehlig, and E. Variano, Phys. Fluids **27**, 035101 (2015).
- [30] K. Gustavsson and B. Mehlig, Advan. Phys. **65**, 1 (2016).
- [31] See Supplemental Material [url], which includes Refs.[39–43], for a full description of the statistical model, for details on the perturbative calculations, and for results on the alignment with vorticity.
- [32] S. Vajedi, K. Gustavsson, B. Mehlig, and L. Biferale, J. Fluid Mech. **798**, 187 (2016).
- [33] D. Bakhuis, V. Mathai, R. A. Verschoof, R. Ezeta, D. Lohse, S. G. Huisman, and C. Sun, Phys. Rev. Fluids **4**, 072301 (2019).
- [34] G. M. Barbara and J. G. Mitchell, FEMS Microbiol Ecol. **43**, 99 (2003).
- [35] R. Stocker and J. R. Seymour, Microbiol. Mol. Biol. Rev. **76**, 792 (2012).
- [36] A. Sokolov, I. S. Aranson, J. O. Kessler, and R. E. Goldstein, Phys. Rev. Lett. **98**, 158102 (2007).
- [37] S. D. Ryan, G. Ariel, and A. Beer, Biophys. J. **111**, 247 (2016).
- [38] C. Dombrowski, L. Cisneros, S. Chatkaew, R. E. Goldstein, and J. O. Kessler, Phys. Rev. Lett. **93**, 098103 (2004).
- [39] G. Falkovich, K. Gawedzki, and M. Vergassola, Rev. Mod. Phys. **73**, 913 (2001).
- [40] K. Gustavsson, M. Z. Sheikh, D. Lopez, A. Naso, A. Pumir, and B. Mehlig, arxiv:1904.00481 (2019).
- [41] U. Frisch, *Turbulence* (Cambridge University Press, Cambridge, UK, 1997) 296p.
- [42] E. Calzavarini, R. Volk, M. Bourgoïn, E. Leveque, J. F. Pinton, and F. Toschi, J. Fluid Mech. **630**, 179 (2009).
- [43] K. Gustavsson and B. Mehlig, Europhys. Lett. **96**, 60012 (2011).